The Japan Society
of Applied Physics

REGULAR PAPER

Terahertz imaging technique for monitoring the flow of buffer solutions at different pH values through a microfluidic chip

View the article online for updates and enhancements.

Terahertz imaging technique for monitoring the flow of buffer solutions at different pH values through a microfluidic chip

Feroz Ahmed[1*] ⬡, Atsuya Mahana[2], Katsuya Taniizumi[2], Jin Wang[2], Kenji Sakai[2], and Toshihiko Kiwa[2*]

[1]Graduate School of Natural Science and Technology, Department of Medical Bioengineering, Okayama University 3-1-1, Tsushima-naka, Kita-ku, Okayama, 700-8530 Japan
[2]Graduate School of Interdisciplinary Science and Engineering in Health Systems, Department of Medical Bioengineering, Okayama University 3-1-1, Tsushimanaka, Kitaku, Okayama, 700-8530 Japan

*E-mail: feroz-ahmed@s.okayama-u.ac.jp; kiwa@okayama-u.ac.jp

Polydimethylsiloxane (PDMS)-based mold prepared using a 3D-printed structure is a cost-effective material and tool to fabricate robust microfluidic chips (MCs) without requiring expensive clean room facilities. A capillary-based MC made of PDMS can be attached onto a glass substrate to visualize the chemical reactions in different types of pH buffer solutions (BSs) flowing through microflow channels (MFCs) using terahertz (THz) image sensing technology. In this study, we designed a microfluidic structure with two inlet wells and an outlet well, equipped with a Si:sapphire substrate to visualize the chemical interaction between BSs injected at different pH values (4 and 10) through an MFC. THz imaging maps were captured during the flow of the BSs using a THz chemical microscope, and the fluid dynamics was studied. We determined and plotted the variation in the THz amplitude data with respect to the BS concentration and analyzed the characteristics of the data.
© 2021 The Japan Society of Applied Physics

1. Introduction

Terahertz (THz) waves are electromagnetic waves with frequency components between 100 GHz and 10 THz, exhibiting unique spectral features such as a non-ionizing nature,[1,2] non-invasiveness,[1,2] penetration[2] capabilities through non-polar molecules, phase-sensitivity to polar substances,[1,3] and high spatial resolution,[1,4] making this a promising technology for applications in spectroscopy,[5,6] sensing,[7] and imaging[8] processes. Therefore, chemical solutions, cells, and tissues with different water contents show distinct responses to THz wave radiation. Moreover, THz imaging can reveal the orientation of a hydrogen bond owing to its intermolecular bonding. When traveling through a medium with a high water concentration, THz radiation gradually diminishes. Therefore, it can be utilized to differentiate even small fluctuations in the water contents of chemical and biological substances such as pH buffer solutions (BSs), tissues,[5] and blood,[9] making THz waves influential for monitoring and identifying the interaction between chemical reactions occurring in different chemical solutions, and abnormal cell divisions inside tissues for cancer cell detection. In comparison, conventional cameras cannot visualize the chemical reactions occurring inside microfluidic chips (MCs).

Compared to using a charge-coupled device camera[10,11] to capture images of the interaction between chemical and biological reactions occurring inside MCs, the application of THz image sensing technology represents the latest advancement in lab-on-chip technology for visualizing, monitoring, and imaging chemical and biological reactions in detail. Thus, the breakthrough of the THz imaging system is prominent for detecting, visualizing, and imaging chemical reactions occurring in BSs maintained at different pH values and flowing without using any fluorescent dye marker, making it a reliable label-free detection[12] and visualization technique. The THz technology is feasible even if microfluidic channels (MFCs) made from different materials are opaque[1,2] in the visible and near-infrared domains, i.e., when they are not transparent under light. For the fabrication of MCs, the choice of materials or extension of the properties of the materials can be realized by testing the effectiveness of this technology over a wide-scale range for advancing chemical and medical research.

Our research group proposed and developed a THz chemical microscope (TCM)[13–16] for a detailed measurement of the chemical reactions occurring in biological and chemical solutions. We demonstrated concanavalin A (con A)–d- (+)-mannose (mannose) interaction using the TCM with mannose applied as an analyte for a detailed analysis of the kinetics of low-molecular-weight molecules.[17] Studies have realized a simultaneous detection of bio-related materials inside a small amount of chemical solution[11,12,18] on a single chip for an early-stage medical diagnosis using the TCM system. The spatial resolution in the case of conventional THz spectroscopy is limited by the wavelength of THz ($\lambda = 300\ \mu$m), whereas the spatial resolution in the case of the TCM system is limited by the wavelength of ultrafast laser pulses ($\lambda = 0.8\ \mu$m). As a result, a small amount of water solution, e.g. less than 16 nl, can be measured[12] using the TCM measurement system. Figure 1 shows a conceptual diagram of our designed MC with the application of THz wave. In Fig. 1, pH 1.68, 4, 6.86, 10 BSs injected through the MC using syringe-connected two tubes.

In this study, a polydimethylsiloxane (PDMS)[19–21]-made capillary design concept based on two inlet wells and one outlet well was fabricated, as shown in Fig. 2(a) and illustrated in Fig. 2(b). We provide a graphical representation of the THz amplitude with respect to different pH concentration data to facilitate the characteristics of the effect of mixing different pH BSs for a quantitative measurement of the pH values. In the final step, we obtain THz image data corresponding to different fluid flow rates[22,23] at two pH values (4 and 10) during the measurement inside the TCM system. Finally, based on the concept of fluid dynamics,[24] during the flow of the BS through an MFC, the effects of the fluid flow patterns through the microfluidic path and the laminar[22,24,25] nature of the mixture of the two
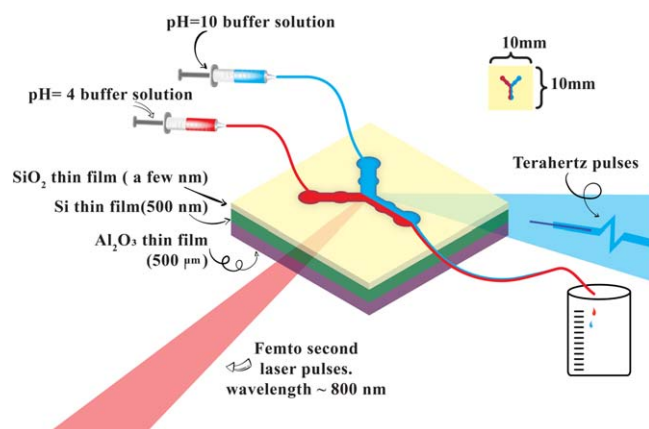
Fig. 1. (Color online) BS solutions at pH values of 4 and 10, injected through two inlets via syringes and flushed out through the outlet with the application of THz electromagnetic waves.

pH BSs are discussed by analyzing the recorded THz imaging data.

2. Experiments

PDMS is frequently used as a substrate material for fabricating lab-on-a-chip and micro total analysis systems.[26] In general, for assembling and fabricating a complete microfluidic system followed by either a reversible or an irreversible process,[26] multiple PDMS components can be used. In this research, we employed a Sylgard® 184 silicone elastomer base agent and a Sylgard® 184 silicone elastomer curing agent as an adhesive, manufactured by Dow Corning (Midland, Maryland, USA), to develop a PDMS-made microfluidic structure following an irreversible assembly process.[26] To prepare the samples, we cross-linked both the base and curing agents at a mass ratio of 10:1. For this purpose, using CAD software, we designed a 3D structure of an MC with two inlet wells and one outlet well (Fig. 2) and printed the structure using a 3D printer in our laboratory.

The two cross-linked base and curing agents were poured into the 3D-printed structure to prepare a replica mold of the 3D structure. The poured solutions were then placed in an oven controlled at a temperature of 40 °C for 24 h to ensure that the replica mold of the MC is sufficiently hard. As shown in Fig. 2(a), the replica mold is cut manually to dimensions of

11 mm × 11 mm to attach it with a sensing chip made of an Si:sapphire substrate (dimensions: 10 mm × 10 mm). The process used for the intensive contact of the MC with the sensing chip was reversible assembly. Subsequently, the MC attached with the sensing chip was clipped onto the middle of the entire sensing plate having dimensions of 40 mm × 40 mm. The sensing chip was utilized to scan the desired biological and chemical reactions using a laser-controlled THz signal. The bottom sensing plate, shown in Fig. 2(a), was screwed to the top plate with dimensions of 40 mm × 40 mm to ensure a tight and intensive contact of the MC, which was sandwiched between the top and bottom sensing plates. Figure 3(a) shows a schematic of the entire process of such an intensive contact. Figure 3(b) shows the three different layers of the sensing chip.

The sensing chip clipped with a sensing plate was used as a sensor, as shown in Figs. 2(a) and 3(b). It consists of three layers of thin films of SiO_2 and Si deposited on a sapphire substrate, as shown in Fig. 3(b). When the silicon layer is illuminated by a femtosecond laser beam from the sapphire substrate side, the electrons in the valence band jump to the conduction band, as shown in Fig. 4. Excitation of an electron into the conduction band occurs because an electron absorbs a photon of the femtosecond laser pulse, whose photon energy is higher than the bandgap energy of silicon. The magnitude of the formed depletion region depends on the electrical potential at the surface of the sensing plate. Thus, we determined the amplitude of the radiated THz waves, which depends on the magnitude of the depletion field. When BSs of different pH values, such as 4 and 10, flowing through the MFCs interact on the sensing plate, the electric potential at the surface of the sensing plate and the amplitude of the radiated THz waves vary.[11] Consequently, a THz electromagnetic wave that is proportional to the differential of the current density by the carrier acceleration[27] is generated according to (1)

$$E_{THz} \propto \frac{dJ}{dt} = e\frac{dn}{dt}\mu E_d S + en\mu\frac{dE_d}{dt}S. \quad (1)$$

In (1), E_{THz} indicates the THz electromagnetic wave, J is the current density, e is the electric charge, n is the photo-excited carrier density, S is the irradiated area of the laser spot, E_d is the surface electric field, and μ is the carrier mobility.
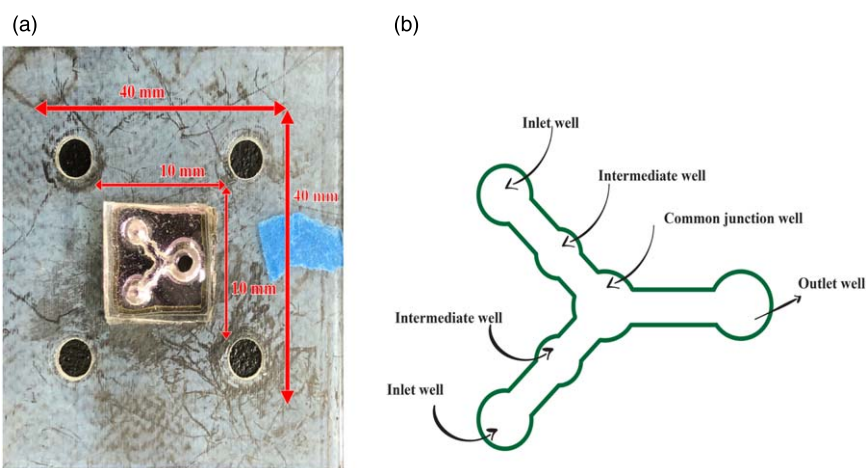

Fig. 2. (Color online) (a) Sensing plate clipped with a Si-sapphire substrate (sensing chip) where the attached MC is at the top. (b) Layout of different dimensional and different patterned wells in the MC.
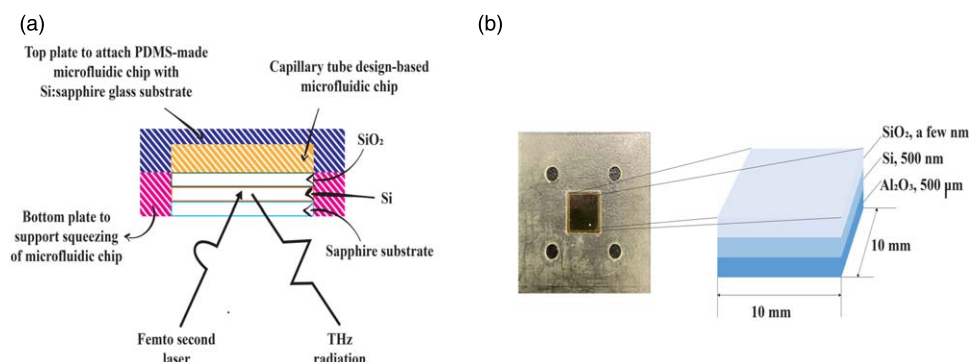
Fig. 3. (Color online) (a) Schematic arrangement of the preparation of sensing plate. (b) Three different layers fabricated sensing chip clipped with the sensing plate.
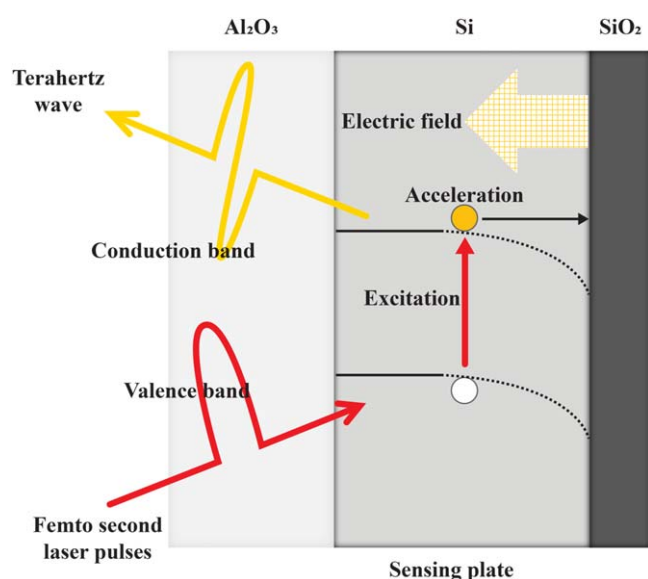

Fig. 4. (Color online) Irradiation of laser pulses onto the layers of the sensing chip to generate THz electromagnetic waves.

Figure 4 illustrates the generation principle of the terahertz waves originating from the sensing plate.

For acidic pH solutions (pH: 4, 1.68, and 6.86), the H^+ ion concentration is higher than the OH^- ion concentration. In comparison, for a BS with a pH of 10, the OH^- ion concentration is higher than the H^+ ion concentration. In each case, both the H^+ and OH^- ions interact with each other to reach chemical equilibrium, leading to a potential shift on the surface of the sensing plate. This leads to changes in the acceleration of the carriers. Therefore, the intensity of the generated terahertz wave also changes, and the interaction between different H^+ and OH^- ion concentrations was measured from the change of the intensity of the THz amplitude.[11] Figure 5 shows the THz detection principle.

To establish a THz signaling system, we used a Ti:sapphire laser as a light source. The center wavelength of the laser pulse was 780 nm with a pulse width of 100 fs at the full width at half maximum. The output of the laser system was 790 W with a repetition rate of 82 MHz.[27,28] We set up a digital pressure machine (DPM) connected to the two inlet wells of the MC via two syringe-connected tubes to allow the flow of BSs with different pH values. The mixed pH solutions, such as pH 4, 1.68, 6.86, and 10, were flushed out naturally and sent to a beaker using another tube from the outlet well. Figure 6 illustrates the experimental setup.

A THz detector was used to detect the amplitude of the THz pulses. We used a bowtie-type photo-conductive antenna as a detector, which was made from a low-temperature-grown GaAs thin film. The peak amplitude of the THz wave was determined from the optical delay of the trigger pulses to the detector, which was fixed. To improve the signal-to-noise ratio of the THz signal, a lock-in technique was applied. We used a chopper (the frequency of the chopper for our system was 2 kHz to synchronize the THz data) in the lock-in technique for reducing the noise from the THz signal data.[27,28] Further, to improve the contrast of the THz images and to sample the THz signal data in a compatible manner
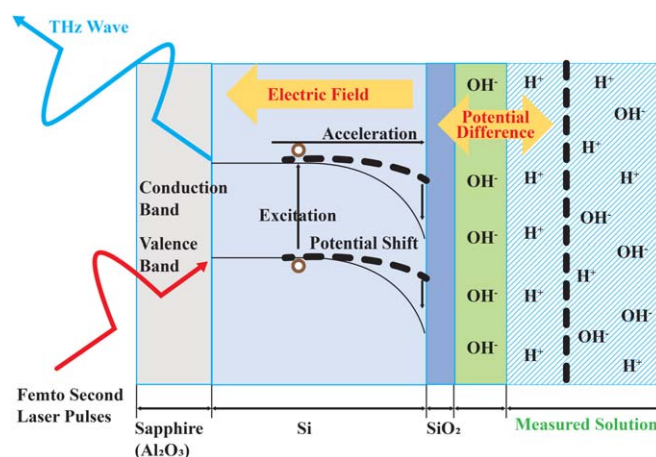

Fig. 5. (Color online) Detection of pH BS interaction using THz electromagnetic waves.
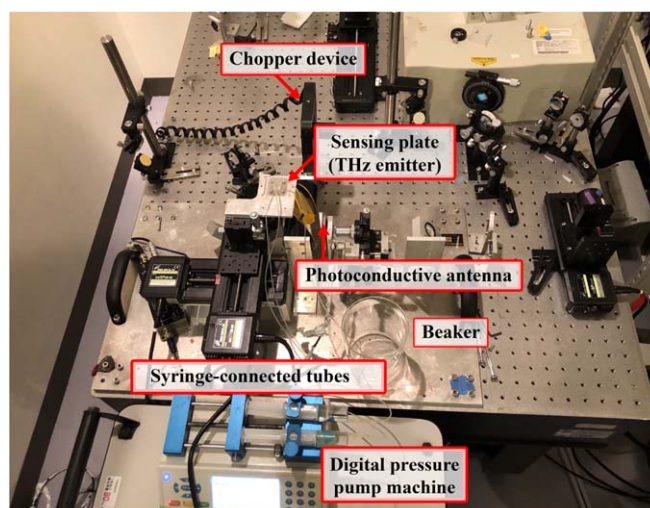
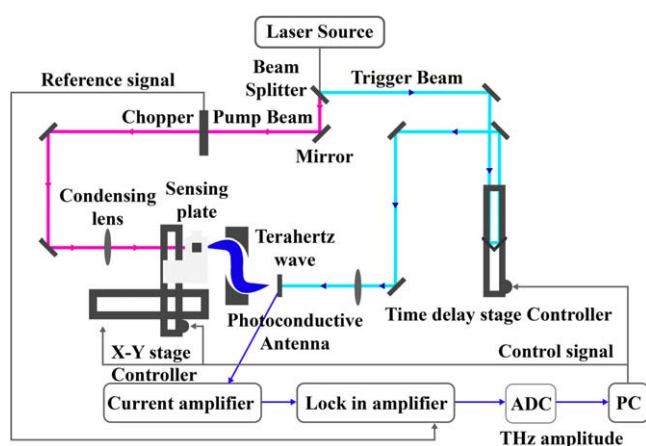**Fig. 6.** (Color online) Optical part of the TCM system.

Fig. 7. (Color online) Entire THz signaling system for the conversion of optical signal to electrical signal with a controlling mechanism.

based on the Nyquist sampling theorem, an adaptive digital filter[28] and an analog-to-digital converter were used by applying a two-stage time delay controlling mechanism[28] in LabVIEW®. The THz signaling system provides results in the form of a signal flow graph, as shown in Fig. 7.

From the experimental average raw data[28] of the contour images of THz, the averaged data of the THz amplitudes as a function of the pH value are plotted in Fig. 8. For this purpose, a laser scanned area of $10\,mm \times 10\,mm$ was

programmed in LabVIEW® to average the lock-in-obtained data over the total measurement time.[28] The characteristic curve indicates the peak values of the THz data, which increased monotonically with the increase in the pH concentration. The negative value of $pH = 1.68$ in Fig. 8 can be explained by the THz generation and detection principles (Figs. 4 and 5), where the potential shift in the depletion region exhibited a downward or reverse shift in the depletion layer, which led to a negative peak value in the THz amplitude data. The sensitivity of our TCM system to pH values revealed quantitative measurements of the pH values through the MFC of the MC. Thus, the interaction of the pH values through the MC can provide a breakthrough to determine even a small variation in the pH level to test the sensitivity for quality assurance, where the use of pH BSs is of great interest.

3. Results

In the experiment, the interaction of two BSs with $pH = 4$ and 10 was captured in the form of THz data and plotted as a contour of the THz images for different fluid flow rates (for example: 0.07, 0.15, 0.25, and 0.4 ml min^{-1}) applied to each of the two inlet wells of the MC as input data, driven by a THz laser-scanned TCM system. In each experimental case, using syringes through two connected tubes, the same set of values of the fluid flow rates from the DPM was applied to each of the two inlet wells. Figures 9 and 10 show the maps
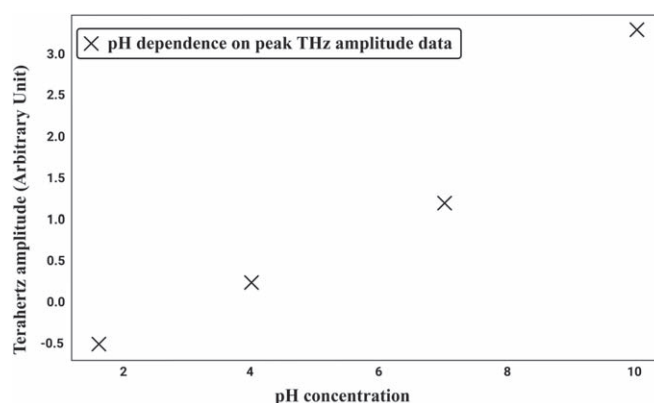

Fig. 8. THz response curve with respect to different pH concentrations.
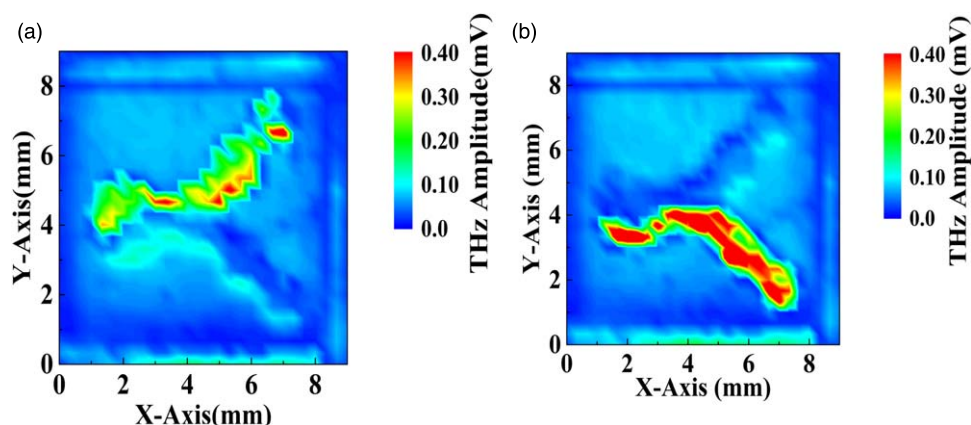
Fig. 9. (Color online) Imaging maps at fluid flow rates of (a) 0.07 ml min^{-1}, and (b) 0.15 ml min^{-1}, both for low and intermediate fluid flow rates of mixed pH 4 and 10 buffer solutions through the MC.
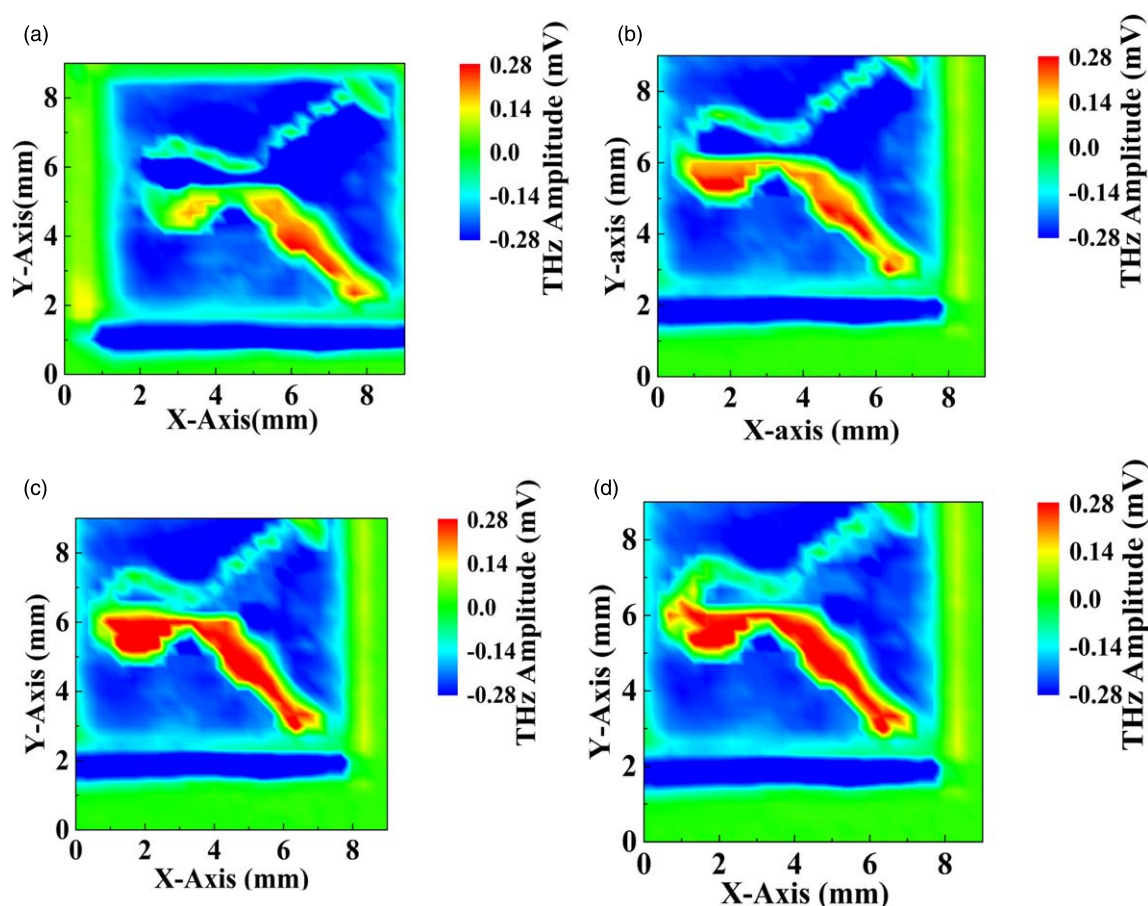

Fig. 10. (Color online) Imaging maps at fluid flow rates of (a) 0.25 ml min^{-1}, (b) 0.4 ml min^{-1}, (c) 0.7 ml min^{-1}, and (d) 0.8 ml min^{-1}. All are intermediate and high fluid flow rates of mixed pH 4 and 10 buffer solutions through the MC.

of the microfluidic reactions occurring in the two pH BSs through the fabricated MFC in the form of THz images. The red, yellowish mixed color indicates the fluid flow patterns for the pH 10 solution in Figs. 9(a) and 9(b) and Figs. 10(a)–10(c). The pH 4 solution showed flow patterns similar to the surface mapping shapes shown in Figs. 9(a) and 9(b) and Figs. 10(a)–10(c).

The red, yellowish colored fluid flow patterns for the pH 10 solution showed maximum flow patterns in most of the flow regimes corresponding to the maximum changes in the intensities of the THz amplitudes of 0.4 mV, as shown in Figs. 9(a) and 9(b), and 0.28 mV in Figs. 10(a)–10(c). In

comparison, the pH 4 solution showed flow patterns similar to the surface mapping shapes corresponding to the change in the minimum intensities of the THz amplitudes from 0 to 0.1 mV in Figs. 9(a) and 9(b) and −0.28 to −0.14 mV in Figs. 10(a)–10(c). The acquisition time[28] was 32 min for 56 700 by 56 700 points in a laser scanned area with a spatial resolution of 333 μm.

In Figs. 9(a) and 9(b) and Figs. 10(a)–10(c), based on the basic concept of fluid dynamics, as two fluidic solutions do not mix with each other when flowing through the internal layers of the flow channels separately, BSs with pH 4 and 10 exhibited an overall laminar fluid flow. Two different viscous

solutions passed through the robust internal surface of the MFC while dragging[22] at the surface walls or boundaries of the flow channels owing to the friction, which in turn slightly deviated the speed[22,23] from the spontaneous flow of the fluidic solutions. The higher the viscosity of the fluid,[22] the higher the tendency of the fluid flow speed to deviate with increasing fluid flow rate. In Figs. 9(a) and 9(b) and Figs. 10(a)–10(c), the measured viscosity of the pH 10 solution in the laboratory (0.58 mPa·s) was higher than that of the pH 4 solution (viscosity of 0.5 mPa·s). Therefore, the pH 10 solution showed a slight frictional dragging effect in that it deflected slightly in the middle or final stages of the fluid flow patterns with the increase in the fluid flow rate in comparison with that of the pH 4 solution. Nevertheless, the combined flow is laminar owing to the nature of the flow patterns in the internal layers given the non-mixing flow nature of BSs with pH 4 and 10 and the consideration of smaller dimensions[29,30] of the MFC of the MC.

The nature of the fluid flow patterns through the MFC from the imaging results has been discussed on the basis of fluid dynamics. It is necessary to identify and analyze the flow patterns of fluids after mixing. Owing to the more stable and calm nature of the fluid flow, it becomes more convenient to trace the fluid flow patterns and evaluate the performance of the designed MC.

4. Conclusion

The microfluidic structure proposed in this study can be used to test tissues and liquid food samples and analyze how a small variation in the pH level can affect the concentrations of the samples by capturing THz images in the form of changes in the intensities of the THz amplitude data. Thus, we can detect an abnormal case of pH-level variation in tissues and food samples and in tablet coatings for an early medical diagnosis of patients, and quality assurances in food and pharmaceutical industries. In addition, from the fluid flow patterns of the THz imaging results, we revealed the laminar nature of the flow of fluids. The laminar nature of the fluid flow as obtained experimentally was confirmed using a 2D fluid dynamics simulation in an ANSYS fluent simulator. We are currently in the process of developing a more complex structural design for MCs, wherein it is possible to flow more than two chemical or biological solutions to facilitate the internal interactions occurring in multiple fluidic solutions for further analyses in the area of lab-on-chip technology.

ORCID iDs

Feroz Ahmed https://orcid.org/0000-0003-2517-072X

1) M. Danciu et al., Materials **12**, 1519 (2019).
2) X. Yang, X. Zhao, K. Yang, Y. Liu, Y. Liu, W. Fu, and Y. Luo, Trends Biotechnol. **34**, 810 (2016).
3) E. Pickwell-MacPherson and V. P. Wallace, Photodiagn. Photodyn. Ther. **6**, 128 (2009).
4) H. H. Nguyen Pham, S. Hisatake, O. V. Minin, T. Nagatsuma, and I. V. Minin, APL Photonics **2**, 056106 (2017).
5) M. He, A. K. Azad, S. Ye, and W. Zhang, Opt. Commun. **259**, 389 (2006).
6) E. P. J. Parrott and J. A. Zeitler, Appl. Spectrosc. **69**, 1 (2015).
7) H. Zhou, C. Yang, D. Hu, D. Li, X. Hui, F. Zhang, and X. Mu, Appl. Phys. Lett. **115**, 143507 (2019).
8) R. I. Stantchev, X. Yu, T. Blu, and E. Pickwell-MacPherson, Nat. Commun. **11**, 2535 (2020).
9) K. Jeong, Y. M. Huh, S. H. Kim, Y. Park, J. H. Son, S. J. Oh, and J. S. Suh, J. Biomed. Opt. **18**, 107008 (2013).
10) R. C. de Sena, M. Soares, M. L. O. Pereira, R. C. D. da Silva, F. F. do Rosário, and J. F. C. da Silva, Sensors **11**, 864 (2011).
11) T. Kiwa, J. Kondo, S. Oka, I. Kawayama, H. Yamada, M. Tonouchi, and K. Tsukada, TRANSDUCERS 2007—2007 Int. Solid-State Sensors, Actuators and Microsystems Conf., 2007, p. 1915.
12) M. Ogawa, A. Nakamura, K. Omura, K. Sakai, T. Kiwa, and K. Tsukada, 2014 XXXIth URSI General Assembly and Scientific Symp. (URSI GASS), 2014, p. 1.
13) T. Kiwa, Y. Kondo, Y. Minami, I. Kawayama, M. Tonouchi, and K. Tsukada, Appl. Phys. Lett. **96**, 211114 (2010).
14) T. Kuwana, M. Ogawa, K. Sakai, T. Kiwa, and K. Tsukada, Appl. Phys. Express **9**, 042401 (2016).
15) T. Kiwa, T. Kamiya, T. Morimoto, K. Sakai, and K. Tsukada, Opt. Express **26**, 8232 (2018).
16) T. Kiwa, K. Sakai, and K. Tsukada, SPIE Newsroom (2013), https://doi.org/10.1117/2.1201312.005281.
17) T. Kiwa, S. Oka, J. Kondo, I. Kawayama, H. Yamada, M. Tonouchi, and K. Tsukada, Jpn. J. Appl. Phys. **46**, L1052 (2007).
18) Y. Maeno, T. Kamiya, T. Kiwa, K. Sakai, and K. Tsukada, 2018 43rd Int. Conf. on Infrared, Millimeter, and Terahertz Waves (IRMMW-THz), 2018, p. 1.
19) C.-W. Tsao, Micromachines **7**, 225 (2016).
20) U. Eduok, O. Faye, and J. Szpunar, Prog. Org. Coat. **111**, 124 (2017).
21) S. O. Catarino, R. O. Rodrigues, D. Pinho, J. M. Miranda, G. Minas, and R. Lima, Micromachines **10**, 593 (2019).
22) P. Peter Urone and R. Hinrichs, *College Physics* (OpenStax, Houston, TX, 2012), Chap. 12.4.
23) P. Peter Urone and R. Hinrichs, *College Physics* (OpenStax, Houston, TX, 2012), Chap. 12.1.
24) W. Moebs, S. J. Ling, and J. Sanny, *University Physics* (OpenStax, Houston, TX, 2016), Vol. 1 Chap. 14.
25) P. K. Kundu et al. (ed.) "Laminar flow," *Fluid Mechanics* (Academic, Boston, MA, 2016) 6th ed., p. 409.
26) C. Bettinger, J. T. Borenstein, and S. L. Tao, *Microfluidic Cell Culture Systems* (Elsevier, Oxford, 2012) 2nd ed., p. 3, Chap. 1.
27) T. Kiwa, T. Kamiya, T. Morimoto, K. Fujiwara, Y. Maeno, Y. Akiwa, M. Iida, T. Kuroda, K. Sakai, and H. Nose, Photonics **6**, 10 (2019).
28) F. Ahmed, T. Kamiya, Y. Maeno, T. Kiwa, K. Sakai, and K. Tsukada, 2019 Int. Conf. on Computer, Communication, Chemical, Materials and Electronic Engineering (IC4ME2), 2019, p. 1.
29) N. Ghorashian, S. K. Gökçe, and A. Ben-Yakar, *Microfluidic Systems for Whole-Animal Screening With C. Elegans* (Wiley, New York, 2016), p. 245, Chap. 10.
30) N. Brandenberg and M. P. Lutolf, *Biology and Engineering of Stem Cell Niches* (Academic, Boston, MA, 2017), p. 429.